

ARTICLE



Extracellular vesicles-transferred SBSN drives glioma aggressiveness by activating NF- κ B via ANXA1-dependent ubiquitination of NEMO

Han Chen^{1,2,11}, Xuhong Chen^{2,3,11}, Zhuojun Zhang^{1,2,11}, Wenhao Bao^{1,2,11}, Zhiqing Gao^{1,2}, Difeng Li^{1,2}, Xiaoyi Xie^{1,2}, Ping Zhou^{1,2}, Chunxiao Yang^{1,2}, Zhongqiu Zhou⁴, Jinyuan Pan⁵, Xiangqin Kuang^{1,2}, Ruiming Tang⁶, Zhengfu Feng⁶, Lihuan Zhou⁶, Dachun Zhu⁷, Jianan Yang^{1,8}, Lan Wang⁹, Hongbiao Huang^{1,2}, Daolin Tang¹⁰, Jinbao Liu^{1,2}✉ and Lili Jiang^{1,2}✉

© The Author(s), under exclusive licence to Springer Nature Limited 2022

Glioma is the most common malignant primary brain tumor with aggressiveness and poor prognosis. Although extracellular vesicles (EVs)-based cell-to-cell communication mediates glioma progression, the key molecular mediators of this process are still not fully understood. Herein, we elucidated an EVs-mediated transfer of suprabasin (SBSN), leading to the aggressiveness and progression of glioma. High levels of SBSN were positively correlated with clinical grade, predicting poor clinical prognosis of patients. Upregulation of SBSN promoted, while silencing of SBSN suppressed tumorigenesis and aggressiveness of glioma cells in vivo. EVs-mediated transfer of SBSN resulted in an increase in SBSN levels, which promoted the aggressiveness of glioma cells by enhancing migration, invasion, and angiogenesis of recipient glioma cells. Mechanistically, SBSN activated NF- κ B signaling by interacting with annexin A1, which further induced Lys63-linked and Met1-linear polyubiquitination of NF- κ B essential modulator (NEMO). In conclusion, the communication of SBSN-containing EVs within glioma cells drives the formation and development of tumors by activating NF- κ B pathway, which may provide potential therapeutic target for clinical intervention in glioma.

Oncogene; <https://doi.org/10.1038/s41388-022-02520-6>

INTRODUCTION

Glioma is the most common malignant primary brain tumor, accounting for 30% of all central nervous system tumors and 75% of all malignant brain tumors [1]. Although current treatment approaches have been significantly improved, the prognosis of patients with glioma is still very poor due to the highly invasive characteristics of glioma. Currently, the median survival time of patients is between 14.6 and 20.5 months, and the 5-year survival rate is approximately 5% [2, 3]. If glioma is not effectively treated, it will inevitably invade surrounding normal brain tissues, leading to brain-occupying lesions and rapid progression of glioma, even early recurrence after surgery. It is important to understand the molecular mechanism of glioma aggressiveness and to identify key target genes for the treatment of glioma patients.

Cell-to-cell communication via extracellular vesicles (EVs) between primary tumor cells and the microenvironment of distant organs contributes to tumor progression [4, 5]. EVs promote intercellular communication and reprogramming of recipient cells by transporting DNA or RNA to the surrounding environment

[6, 7]. In addition to nucleotides, tumor cells also communicate with neighboring cells through exosomal releasing proteins to regulate tumor progression, angiogenesis, and metastasis [8, 9]. Although EVs-mediated interactions between glioma cells and non-glioma brain cells shape the tumor microenvironment, the key mediators of this process are still unclear [10].

The nuclear factor kappa-B (NF- κ B) pathway is involved in many biological processes, such as inflammation, immunity, and development, as well as anti-apoptotic properties, angiogenesis, and cell adhesion [11, 12]. NF- κ B also plays a complex role in tumor biology and participates in the formation of hallmarks of cancer [13, 14]. The NF- κ B signaling promotes the aggressiveness and progression of glioma, in which ubiquitination plays an important role in regulating NF- κ B activation [15, 16]. The first step of NF- κ B activation involves in the assembly of a tumor necrosis factor receptor type 1 (TNFR1)-associated signaling complex, which is composed of TNF receptor-associated death domain (TRADD), receptor-interacting protein kinase 1 (RIP1), TNF receptor-associated factors (TRAFs), the E3 ubiquitin ligases

¹Affiliated Cancer Hospital & Institute of Guangzhou Medical University, Guangzhou 510095, China. ²Guangzhou Municipal and Guangdong Provincial Key Laboratory of Protein Modification and Degradation, School of Basic Medical Science, Guangzhou Medical University, Guangzhou 511436, China. ³Medical Research Center, Southern University of Science and Technology Hospital, Shenzhen 518055, China. ⁴Meishan Women and Children's Hospital, Alliance Hospital of West China Second University Hospital, Sichuan University, Meishan 620000, China. ⁵Department of oncology, Huanggang Central Hospital of Yangtze University, Huanggang 438000, China. ⁶The Sixth Affiliated Hospital of Guangzhou Medical University, Qingyuan People's Hospital, Guangzhou 511518, China. ⁷Department of Operating Room, Shenzhen Baoan Women's and Children's Hospital, Shenzhen 518000, China. ⁸Department of Urologic Oncosurgery, Affiliated Cancer Hospital & Institute of Guangzhou Medical University, Guangzhou 510095, China. ⁹Department of Pathogen Biology and Immunology, School of Basic Courses, Guangdong Pharmaceutical University, Guangzhou 510006, China. ¹⁰Department of Surgery, UT Southwestern Medical Center, Dallas, TX 75390, USA. ¹¹These authors contributed equally: Han Chen, Xuhong Chen, Zhuojun Zhang, Wenhao Bao. ✉email: jlili@gzhmu.edu.cn; jiu@gzhmu.edu.cn

Received: 26 April 2022 Revised: 16 October 2022 Accepted: 17 October 2022

Published online: 31 October 2022

cellular inhibitor of apoptosis protein (cIAP) 1, and cIAP2. cIAPs then conjugate K63-linked ubiquitin chains to RIP, leading to the recruitment of the kinase transforming growth factor beta-activated kinase 1 (TAK1) and linear ubiquitin chains assembly complex (LUBAC) followed with Lys63-linked and Met1-linear polyubiquitination of NF- κ B essential modulator (NEMO) [16]. TAK1 mediates I κ B Kinase (IKK) phosphorylation, resulting in IKK activation, and finally inhibitor of κ B (I κ B) α degradation and NF- κ B activation [17]. This highly regulated NF- κ B pathway provides an opportunity to treat cancer.

The suprabasin (SBSN) is a newly identified gene, mainly expressed in differentiated keratinocytes of mice and humans [18]. The upregulated SBSN promotes malignant progression of tumors [19]. SBSN is identified as a secreted protein that can be detected in patient serum [20–22]; however, the release and activity of SBSN in tumor microenvironment is still unknown. In this study, we provide first evidence that EVs mediate the transport of SBSN protein between cells and cause glioma progression by activating NF- κ B signaling pathway. In addition to defining the extracellular functions of SBSN in regulating ubiquitination of NEMO, our clinical studies further show that SBSN is a biomarker that may predict poor prognosis of patients with glioma. These findings highlight that SBSN is a potential therapeutic target for glioma.

RESULTS

SBSN is upregulated in glioma tissues and predicts poor prognosis

To determine the clinical significance of SBSN in glioma, we used IHC staining to examine the expression level of SBSN in commercial glioma tissue microarrays. Compared with normal brain tissue, the expression of SBSN increased in glioma tissues, and the expression in high-grade tumors (WHO grade III + IV) was significantly higher than that in low-grade tumors (WHO grade I + II), which was consistent with the analysis using the TCGA database (Fig. 1A and Supplementary Fig. 1A). Notably, the high expression ratio of SBSN in glioma tissues was positively correlated with the staining index (SI, cutoff by $SI \geq 8$) of low to high grade (Fig. 1B). The expression of SBSN in different histological subtypes of the TCGA database was also examined. This analysis found that compared with other types of gliomas, SBSN was significantly upregulated in glioblastoma multiforme (GBM) which is the subtype with the highest malignancy and the worst prognosis (Supplementary Fig. 1A). In addition, the expression of SBSN was higher in isocitrate dehydrogenase (IDH) wild-type group compared to IDH mutant group in WHO grade IV, indicating a potential correlation between SBSN expression and primary GBM incidence ($P = 0.029$, Supplementary Fig. 1B).

We studied the clinical correlation between the expression level of SBSN and the clinicopathological characteristics of patients with glioma, and confirmed that the overexpression of SBSN was positively correlated with the WHO classification (Fig. 1A and Supplementary Table 2). To clarify the diagnostic value of SBSN in glioma patients, the ROC curve was made. We found that SBSN expression could distinguish glioma patients from healthy controls with an AUC of 0.895 (95% CI: 0.817–0.974; $P = 0.001$). The cutoff value of the mean optical density (MOD) was 16.59, at the highest Youden Index (YI, Sensitivity + Specificity - 1 = 72.02), with a sensitivity of 88.69% and a specificity of 83.33% (Fig. 1C). It also suggested that SBSN expression could distinguish patients with high-grade tumors (III + IV) from low-grade tumors (I + II) with an AUC of 0.917 (95% CI: 0.865–0.968; $P < 0.001$). The cutoff value of MOD at the highest YI was 52.76, with a sensitivity of 85.71% and a specificity of 93.88% (Fig. 1C). Moreover, SBSN expression could indicate patients' mortality with an AUC of 0.820 (95% CI: 0.751–0.888; $P < 0.001$), and predicted the recurrence risk of patients with an AUC of 0.786 (95% CI: 0.712–0.850; $P < 0.001$) (Fig.

1D). These results highlight the possible value of SBSN in glioma diagnosis and assessment of progression status.

Compared with patients with lower SBSN expression, patients with higher SBSN expression had shorter overall and relapse-free survivals (Fig. 1E). This notion was further validated in multiple publicly available glioma datasets (Supplementary Fig. 1C, D). In-depth investigation of the prognostic significance of SBSN in different grades of glioma subgroups showed that high SBSN expression predicted poor overall and relapse-free survivals in the low-grade tumors (I + II) and high-grade tumors (III + IV) subgroup (Fig. 1F), even in the specific separate grade II, III, or IV subgroup (Supplementary Fig. 1E–G). Meanwhile, the univariate and multivariate Cox-regression analysis revealed that the expression level of SBSN was an independent prognostic factor in glioma (Supplementary Table 3). Collectively, these findings indicate that the overexpression of SBSN is closely related to the poor prognosis of patients with glioma.

SBSN mediates glioma aggressiveness in vivo and in vitro

GSEA analysis showed that SBSN expression was positively correlated with gene characteristics of tumor migration (Supplementary Fig. 2A), indicating that SBSN might promote glioma aggressiveness. Next, we used an orthotopic tumor model to assess the role of SBSN in glioma aggressiveness. The murine glioma cells GL261 with SBSN overexpression or knockdown (Supplementary Fig. 2B, C) were stereotactically implanted into the brains of mice. H&E staining showed that control cells generally formed moderately invasive intracranial tumors with relatively visible peritumoral boundaries, while tumors formed by the SBSN-transduced glioma cells exhibited a highly invasive morphology with the borders displaying a palisading pattern of tumor cell distribution and forming spike-like structures and tumor foci invading into the surrounding regions. In contrast, SBSN-silenced cells formed noninvasive, oval-shaped intracranial tumors with sharp edges when expanding as spheroids, compared with control cells (Fig. 2A). Meanwhile, the cells were subcutaneously administered into mice. The tumors formed by SBSN-overexpressed GL261 cells retained a higher growth rate in both size and weight, while the mice inoculated with the SBSN-silencing cells showed smaller and lighter tumor tissues than the control group (Fig. 2B, C). Consistently, the results showed that tumor tissues in the SBSN overexpression group performed spine-like structures and penetrated into the surrounding tissues representing more invasive capacity of glioma cells, while tumor tissues in SBSN low-expression group showed well-defined boundaries, indicating low capacity of local invasiveness (Fig. 2D).

We also found higher density of microvascular in both orthotopic and subcutaneous tumor tissues with overexpression of SBSN, indicating promotion of angiogenesis by SBSN. GSEA analysis showed that SBSN expression was positively correlated with gene characteristics of angiogenesis (Supplementary Fig. 2D). It was confirmed that microvascular outgrowth and microvascular densities (MVD) reflected by the intensity of CD31 staining were enhanced in SBSN-transduced tumors, and reduced in SBSN-silencing tumors ($P < 0.01$, Fig. 2E).

SBSN expression was upregulated in most glioma cells lines based on analysis of the Cancer Cell Line Encyclopedia (CCLE) database (Supplementary Fig. 2E). Furthermore, it was confirmed that SBSN was differentially upregulated in our collected eight glioma cancer cells compared with a normal human astrocyte (NHA) cell (Supplementary Fig. 2F). We then stably overexpressed or silenced SBSN expression in two cell lines A172 and U87MG with moderate levels of SBSN (Supplementary Fig. 2G). Functionally, the overexpression of SBSN increased, while the downregulation of SBSN decreased glioma cells proliferation (Supplementary Fig. 3A). Wound healing assay and transwell assay revealed that overexpression of SBSN enhanced, while downregulation of SBSN limited the migration and invasion ability of glioma cells (Fig. 3A, B

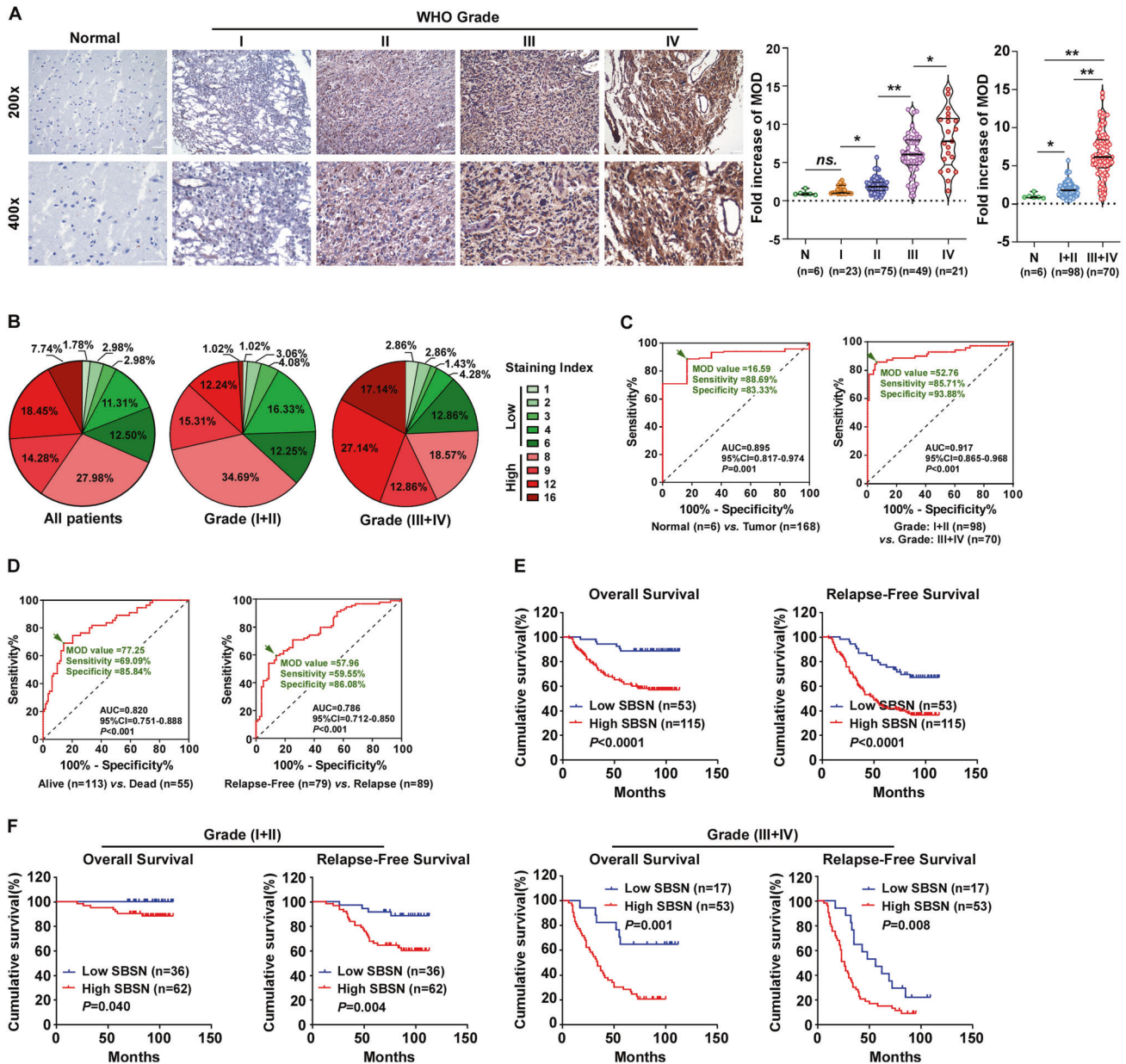


Fig. 1 SBSN is upregulated in glioma and associates with glioma progression. **A** Representative images of IHC analyses of formalin-fixed paraffin-embedded glioma specimens compared with normal brain tissue. Scale bar, 20 μm; statistical quantification of the mean optical density (MOD) of SBSN staining (right). **B** Distribution of SBSN staining index (SI). The SI 8 was chosen as the cutoff value and SI ≥ 8 was considered as high expression. **C** ROC curve analysis of SBSN in glioma patients vs. the normal control, and in high-grade glioma (III + IV) vs. low-grade glioma (I + II). **D** ROC curve analysis of SBSN in glioma patients alive vs. dead, and in patients with relapse vs. relapse-free status. **E** Kaplan–Meier analysis of overall survival (left) and relapse-free survival (right) of 168 patients with glioma with low vs. high expression of SBSN. **F** Kaplan–Meier analysis of overall survival and relapse-free survival for patients in the clinical low-grade and high-grade glioma subgroups. *P* values were calculated by using the log-rank test. **P* < 0.05. ***P* < 0.01.

and Supplementary Fig. 3B). Similar results were obtained in two other cell lines, LN229 and T98G (Supplementary Figs. 2G and 3C). In a 3-D invasive culture assay, SBSN-overexpressing glioma cells displayed the typical morphology of highly aggressive cells, presenting more outward projections than control cells; in contrast, the SBSN-knockdown glioma cells showed spheroid morphologies and less projections (Fig. 3C). The angiogenesis function was further determined using HUVECs. Remarkably, ectopic expression of SBSN promoted, and SBSN inhibition attenuated the ability of glioma cells to induce tube formation and migration of HUVECs (Fig. 3D and Supplementary Fig. 3D). These results demonstrate that SBSN promotes aggressiveness of glioma.

EVs-mediated transfer of SBSN promotes glioma aggressiveness

Heterogeneity is a key feature of glioma and leading to aggressiveness of glioma and poor prognosis of patients [23, 24]. As expected, the values of MOD used to determine the quantification of the IHC staining in the same tissue were scattered obviously, with a mean of 0.288 and a range of 0.156–0.500 in tissue of P1 (Grade II), and a mean of 0.408 and a range of 0.229–0.648 in tissue of P2 (Grade III), and a mean of 0.536 and a range of 0.301–0.807 in tissue of P3 (Grade IV) (Supplementary Fig. 4A). These findings show that different tumor cell subsets have different degrees of staining intensity within the

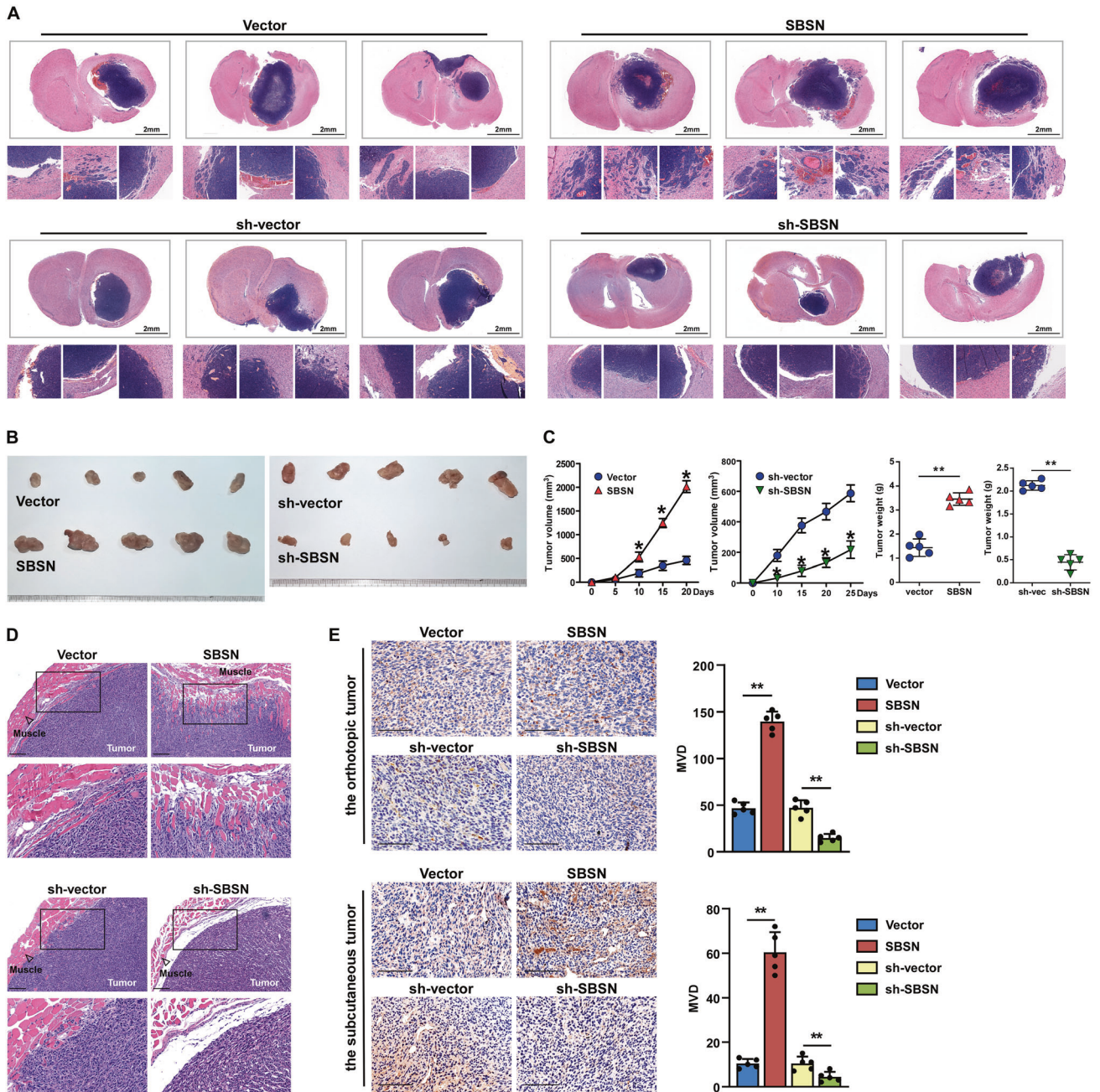


Fig. 2 SBSN enhances glioma aggressiveness in vivo. **A** H&E staining of the orthotopic tumors from indicated group. The indicated cells were intracranially injected into the brain of mice. Scale bar, 2 mm. **B** Representative images of subcutaneous tumors. **C** The tumor volumes and weights. **D** H&E staining of subcutaneous tumors from indicated group. Scale bar, 300 μ m. **E** Representative image and quantification of MVD in orthotopic and subcutaneous tumors indicated by CD31 staining. Scale bar, 100 μ m. GL261 cells were used for the in vivo experiments.

same tissue sample, supporting that gliomas have a high degree of tumor heterogeneity. We further explored whether cell-to-cell communication exists between these heterogeneous tumor cells, and the manner and subsequent outcomes. Given that SBSN can act as a secreted protein [20–22], which may make it a potential carrier for intercellular communication, we first investigated the effect of secreted SBSN on glioma cells within tumor environment. Overexpression of SBSN through gene transfection not only increased endogenous expression of SBSN, but also caused its secretion in the supernatant of U87MG cells; in contrast, the deletion of secretion signaling peptide of SBSN (SBSN-OPT) markedly reduced its secretion (Supplementary Fig. 4B, C).

Strikingly, the conditioned medium (CM) from SBSN-OPT group could incompletely reduce the invasion ability of recipient U87MG cells (Fig. 4A). Moreover, the recipient U87MG cells treated with the CM from SBSN-overexpressed cells exhibited increased levels of SBSN, whereas the CM from SBSN-silencing cells displayed reduced SBSN expression in the recipient cells (Fig. 4B). All these results suggested that some other secretory mechanisms may play a role in the transfer of SBSN between glioma cells.

We focused on EVs due to their roles of cell communication by transporting oncogenic driver factors [25, 26]. The FunRich cluster analysis of the mass spectrometry revealed that EVs-related proteins were highly enriched in the supernatants of SBSN-

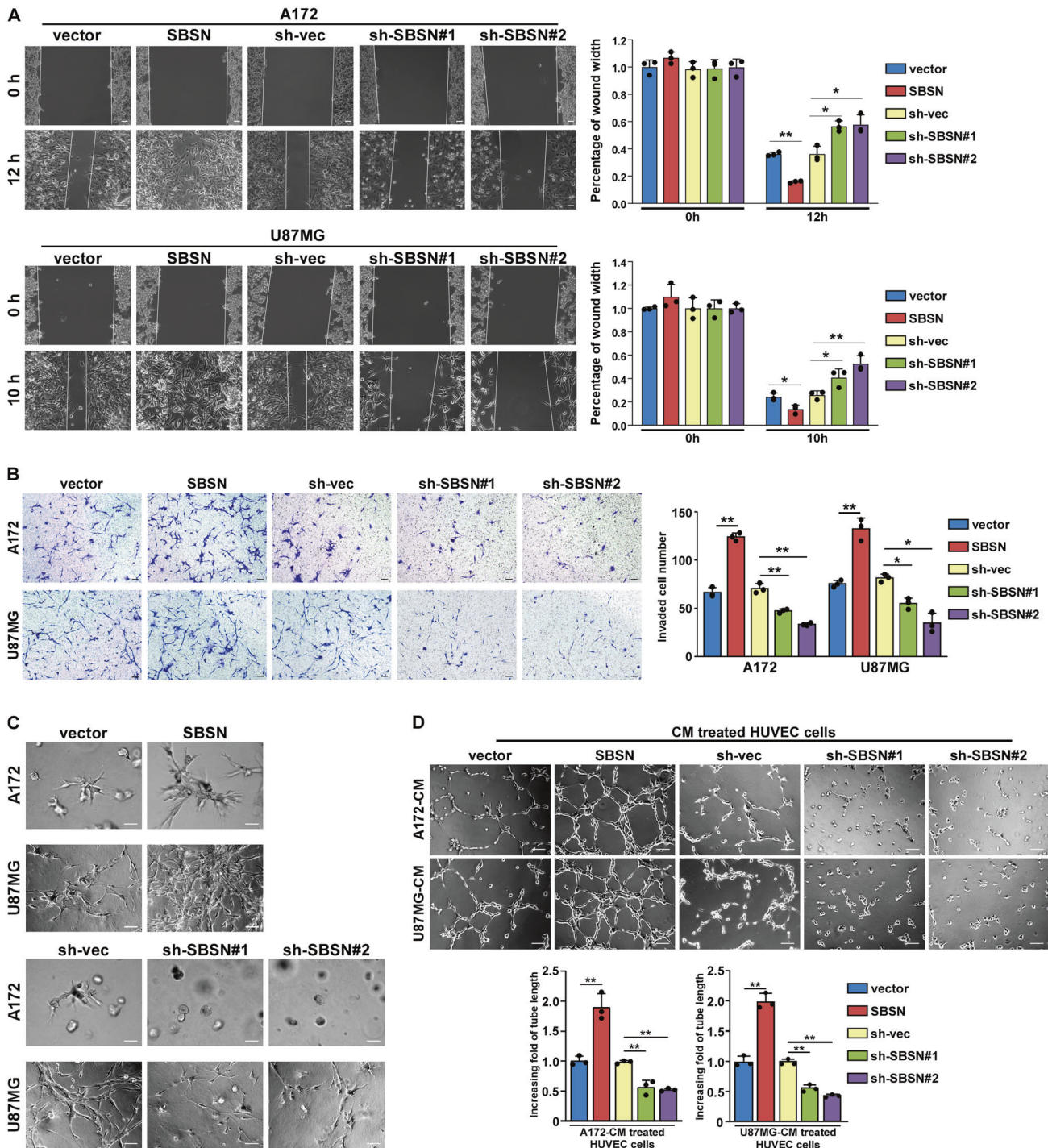


Fig. 3 SBSN enhances glioma aggressiveness in vitro. **A** Wound healing assay of the indicated cells. Scale bar, 20 μ m. **B** Representative images (left) and quantification (right) of indicated invaded cells analyzed in a transwell matrix penetration assay. Scale bar, 20 μ m. **C** Representative micrographs of indicated cells cultured in a 3-D spheroid invasion assay. Scale bar, 50 μ m. **D** Representative images and quantification of tubules formed by HUVECs cultured on BME-coated plates with conditioned medium (CM) from indicated glioma cells. Scale bar, 20 μ m. A172 and U87 cells were used for the in vitro experiments. sh-vec: shRNA-vector, sh-SBSN: shRNA-SBSN. Error bar represents the mean \pm SD of three independent experiments. * $P < 0.05$; ** $P < 0.01$.

overexpressing U87MG cells and SBSN-interacting proteins profiles (Fig. 4C). The nanoparticle tracking analysis (NTA) and western blotting analysis showed that all EVs isolated from different SBSN expression groups using ultracentrifugation were within the expected size range (40–150 nm) (Fig. 4D and Supplementary Fig. 4D) and contained specific EVs marker proteins CD9 and CD63, but the absence of calnexin (Fig. 4E

and Supplementary Fig. 4E). To confirm the cell-entering ability of EVs, EVs were isolated and then pre-labeled by PKH26 lipophilic membrane red fluorescent dye. After the recipient U87MG cells were mixed with PKH26-labeled EVs and incubated for 48 h, the PKH26-labeled EVs derived from parental cells could be effectively taken up by the recipient cells (Fig. 4F). Furthermore, the EVs from parental U87MG cells transfected with the XPack cloning that is

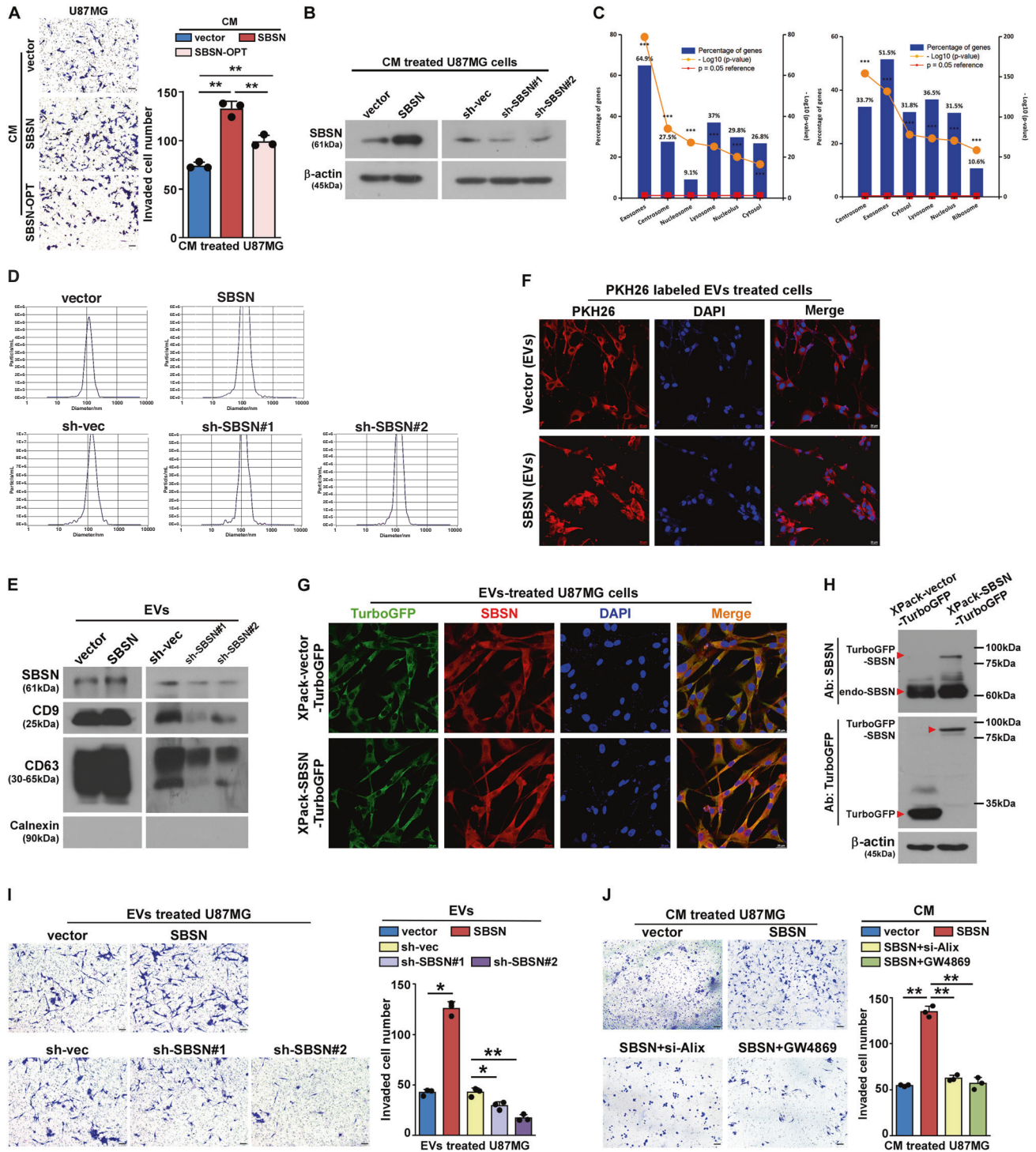


Fig. 4 EVs-transferred SBSN promotes glioma aggressiveness. **A** Representative images (left) and quantification (right) of indicated invaded cells analyzed in a transwell matrix penetration assay after treated with indicated CM. Scale bar, 20 μ m. **B** Western blotting analysis of SBSN protein level in U87MG cells after treated with indicated CM. **C** Cellular component analysis by FunRich for the secreted protein upregulated in SBSN-overexpressing U87MG cells (left), and the IP binding protein of SBSN. Y axis represents percentage of genes (left) or and $-\log_{10}$ (P value) (right). **D** Size distributions of EVs from U87MG cells were measured using NTA analysis. **E** Western blotting analysis of SBSN and EVs markers including CD9, CD63, and calnexin; EVs collected from U87MG cells co-cultured with PKH26-labeled exosomes without EVs used as a dye-fluorescence background control. Scale bar, 20 μ m. **F** Fluorescence microscope images of U87MG cells co-cultured with PKH26-labeled EVs without EVs used as a dye-fluorescence background control. Scale bar, 20 μ m. **G** Fluorescence microscope images of U87MG cells co-cultured with EVs from XPack-vector-TurboGFP and XPack-SBSN-TurboGFP transduced U87MG cells. Scale bar, 20 μ m. **H** The expression of SBSN (including SBSN fused with TurboGFP and endogenous SBSN) and TurboGFP (including TurboGFP and TurboGFP fused with SBSN) were analyzed using western blotting and β -actin served as a loading control. **I**, **J** Representative images (left) and quantification (right) of indicated invaded cells analyzed in a transwell matrix penetration assay after treated with indicated EVs (**I**) or CM from U87MG cells transfected with si-Alix or CM added with EVs inhibitor GW4869 (**J**). Scale bar, 20 μ m. sh-vec: shRNA-vector, sh-SBSN: shRNA-SBSN. Error bar represents the mean \pm SD of three independent experiments. * P < 0.05; ** P < 0.01.

used to load SBSN protein into EVs of glioma cells were taken up by the recipient cells (Fig. 4G). It is further confirmed that EVs from SBSN-overexpressed glioma cells delivered SBSN protein into the recipient cells by western blotting analysis (Fig. 4H).

Subsequent functional assays showed that the invasion and migration abilities of the recipient cells were enhanced by the EVs from SBSN-overexpressed glioma cells (Fig. 4I and Supplementary Fig. 4F). This process was blocked by genetic or pharmacologic inhibition of EVs (ALIX-siRNA or GW4869) (Fig. 4J and Supplementary Fig. 4G). Overall, these findings indicate that EVs-mediated cell-to-cell SBSN transport promotes the aggressiveness of glioma.

EVs-transferred SBSN-mediated NF- κ B activation favors glioma aggressiveness

The GSEA analysis found SBSN expression was positively correlated with the NF- κ B-activated gene signatures (Supplementary Fig. 5A), indicating SBSN might be involved in NF- κ B activation. Luciferase reporter assay revealed that ectopic expression of SBSN enhanced, but silencing SBSN attenuated NF- κ B-induced luciferase activity in glioma cells (Fig. 5A). Constitutive activation of NF- κ B may vary as tumor cell lines are derived from glioma patients with different genetic backgrounds [27, 28]. Consistent with previous studies [29, 30], we also observed distinct constitutive activation of NF- κ B in A172 and U87MG cell lines. Two more cell lines, LN229 and T98G, were added to replicate the experiment and showed consistent results (Supplementary Fig. 5B). Subsequent immunofluorescence staining and subcellular fractionation assays showed that overexpression of SBSN promoted, while knockdown of SBSN attenuated, nuclear translocation of NF- κ B/p65 (Fig. 5B and Supplementary Fig. 5C). The qPCR analysis of NF- κ B target genes also confirmed that SBSN activated NF- κ B (Fig. 5C). Western blotting analysis showed that the phosphorylation levels of IKK α / β , I κ B α and p65 were positively related to the expression of SBSN, whereas SBSN had no significant effect on the expression of total protein of IKK α / β , I κ B α and p65 (Fig. 5D).

To confirm whether NF- κ B activation is required for SBSN-induced glioma aggressiveness, the inhibitors of NF- κ B pathway, including JSH-23 and QNZ, were used *in vitro*. JSH-23 and QNZ abrogated the effects of SBSN overexpression on NF- κ B activation, and the migratory and invasive capability of glioma cells, by detecting the expression of matrix metalloproteinase 9 (MMP9), a tumor invasion marker and NF- κ B target gene of various cancers including glioma [31, 32]) (Fig. 5E, F and Supplementary Fig. 5D, E). Similar results were performed by IKK β silencing, in which the effects of SBSN overexpression on NF- κ B activation and invasive capability of glioma cells were abrogated by IKK β silencing (Supplementary Fig. 5F–H).

The activity of NF- κ B in the recipient glioma cells was enhanced by the EVs produced from SBSN-overexpressed cells (Fig. 5G and Supplementary Fig. 5I). This EVs-mediated NF- κ B activation was reversed by silencing ALIX or using GW4869 (Fig. 5H). Thus, EVs-transferred SBSN promotes glioma aggressiveness by activating NF- κ B signaling. Both orthotopic and subcutaneous mouse tumor tissues with overexpressed SBSN exhibited increased, while SBSN-silenced tumors displayed lower nuclear NF- κ B expression and MMP9 levels (Fig. 5I and Supplementary Fig. 5J). These studies confirm the role of SBSN in activating NF- κ B and glioma aggressiveness, including invasiveness and angiogenesis.

EVs-transferred SBSN activates NF- κ B through ANXA1-dependent NEMO ubiquitination

To further investigate the specific mechanism responsible for SBSN-induced NF- κ B activation, mass spectrum analysis was carried out to identify potential SBSN-interacting proteins. Two NF- κ B signaling-related proteins were identified, namely elongation factor 1-alpha 1 (EEF1A1) [33] and annexin A1 (ANXA1) [34]

(Fig. 6A). Unlike the inhibition of EEF1A1, the knockdown of ANXA1 limited NF- κ B activation in SBSN-overexpressed glioma cells (Fig. 6B and Supplementary Fig. 6A). Western blotting analysis of phosphorylation levels of IKK α / β , I κ B α , and p65 further confirmed the role of ANXA1 in activating NF- κ B signaling (Fig. 6C). The immunofluorescence staining and co-immunoprecipitation (Co-IP) analysis showed that SBSN interacted with ANXA1 and NEMO (Fig. 6D, E). However, the expression of SBSN had no effect on the expression of NEMO and ANXA1 (Fig. 6C and Supplementary Fig. 6B). Furthermore, downregulation of ANXA1, but not EEF1A1, significantly eliminated the enhancement of SBSN overexpression on invasion and migration of glioma cells, further suggesting that ANXA1 is a mediator of SBSN-inducing glioma aggressiveness (Fig. 6F, G and Supplementary Fig. 6C).

Polyubiquitination of NEMO plays a critical role in the assembly of the IKK complex and the subsequent activation of NF- κ B, including Lys63-linked polyubiquitination (K63-Ub) and Met1-linear polyubiquitination (M1-Ub). M1-Ub has stronger affinity to the linear ubiquitin chain generated by LUBAC complex consisting of the heme-oxidized IRP2 ubiquitin ligase-1L (HOIL-1L), HOIL-1L-interacting protein (HOIP), and shank-associated RH domain interactor (SHARPIN) subunits [35, 36]. Overexpression of SBSN increased the levels of HOIL-1, HOIP, and SHARPIN, and elevated the levels of K63-Ub and M1-Ub in glioma cells, while the knockdown of SBSN displayed opposite effects on these events (Fig. 7A). Critically, silencing ANXA1 remarkably abrogated the enhancement of K63-Ub, M1-Ub and LUBAC complex by SBSN overexpression (Fig. 7A). Co-IP analysis further observed that upregulating SBSN increased, while silencing SBSN reduced K63-Ub and M1-Ub levels of NEMO in the precipitate pellets (Fig. 7B and Supplementary Fig. 7A). Moreover, suppression of ANXA1 attenuated the ubiquitin-inducing role of SBSN in NEMO (Fig. 7B and Supplementary Fig. 7B). These assays dissect the role of SBSN in the regulation of NEMO ubiquitination through ANXA1. Moreover, Co-IP analysis confirmed that the EVs from SBSN-overexpressed cells increased K63-Ub and M1-Ub levels of NEMO in the precipitate pellets of the recipient cells (Fig. 7C and Supplementary Fig. 7C). Thus, EVs-transferred SBSN activates NF- κ B through K63 and M1 ubiquitination of NEMO in glioma cells.

DISCUSSION

Ubiquitination regulation of NF- κ B signaling is a striking therapeutic target for cancer [36–38]. In this study, we established a new model of NF- κ B activation in glioma cells through EVs-driven SBSN. Specially, SBSN recruits ANXA1 to trigger K63- and M1-Ub of NEMO, thereby promoting NF- κ B activation and driving glioma aggressiveness (Fig. 7D). Combined with clinical sample analysis and animal experiments, our findings might provide new opportunities for the treatment of glioma.

NEMO is a ubiquitin-binding protein and a target for ubiquitination in the classic NF- κ B signaling pathway. It activates NF- κ B signaling by combining K63 with a linear ubiquitin chain, and the activation of NF- κ B is downregulated when the NEMO ubiquitin-binding region is mutated [37, 39]. Although Ubc13 encodes an ubiquitin conjugating enzyme that is essential for the production of the K63 linker, it has little effect on NF- κ B activation [40], highlighting that NEMO could also activate NF- κ B signaling in a K63-independent ubiquitination manner. Indeed, M1-Ub may mediate NF- κ B activation in a K63-independent manner [41]. Due to the linear ubiquitin chain produced by LUBAC, the binding capacity of M1-Ub to NEMO ubiquitin motif is 100 times higher than that of K63-Ub [36, 42]. In the absence of HOIL-1, one of the LUBAC subunits, the NF- κ B activation is severely impaired [43]. Inhibition of another LUBAC subunit HOIP also increases chemotherapy-induced apoptosis [44]. We not only found that upregulating SBSN increased the K63-Ub level of NEMO in glioma cells, but also revealed that SBSN enhanced the M1-Ub level of

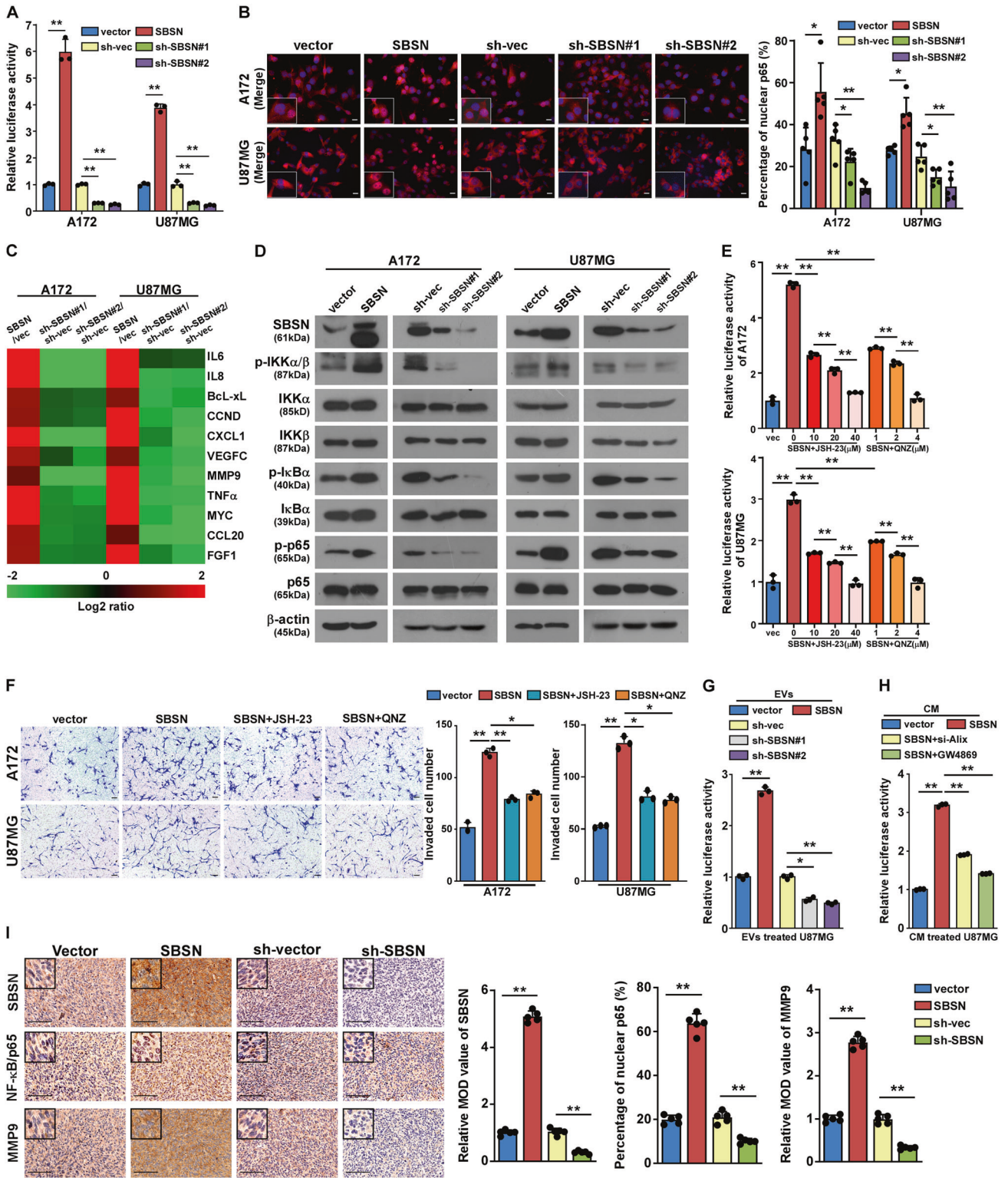


Fig. 5 EVs-transferred SBSN activates NF-κB signaling pathway. **A** NF-κB luciferase reporter activity was analyzed in the indicated cells. **B** Immunofluorescence staining analysis and quantification of subcellular localization of NF-κB/p65 in the indicated cells; images merged p65 with DAPI were shown. Scale bar, 20 μm. **C** qPCR analysis of NF-κB-regulated genes in the indicated cells. **D** Western blotting analysis of NF-κB signaling-related proteins in the indicated cells. **E** NF-κB luciferase reporter activity was analyzed in the indicated cells after treated with indicated dose of NF-κB inhibitor, JSH-23 or QNZ, for 48 h. **F** Representative images (left) and quantification (right) of indicated cells analyzed in a transwell matrix penetration assay after treated with JSH-23 (20 μM) and QNZ (2 μM) for 48 h. Scale bar, 20 μm. **G**, **H** NF-κB luciferase reporter activity was analyzed in the glioma cells treated with indicated EVs (**G**) or CM with si-Alix or GW4869 (**H**). **I** IHC staining (SBSN, NF-κB/p65, MMP9) of the orthotopic tumors from indicated group. Scale bar, 100 μm. vec: vector, sh-vec: shRNA-vector, sh-SBSN: shRNA-SBSN. Error bar represents the mean ± SD of three independent experiments. **P* < 0.05; ***P* < 0.01.

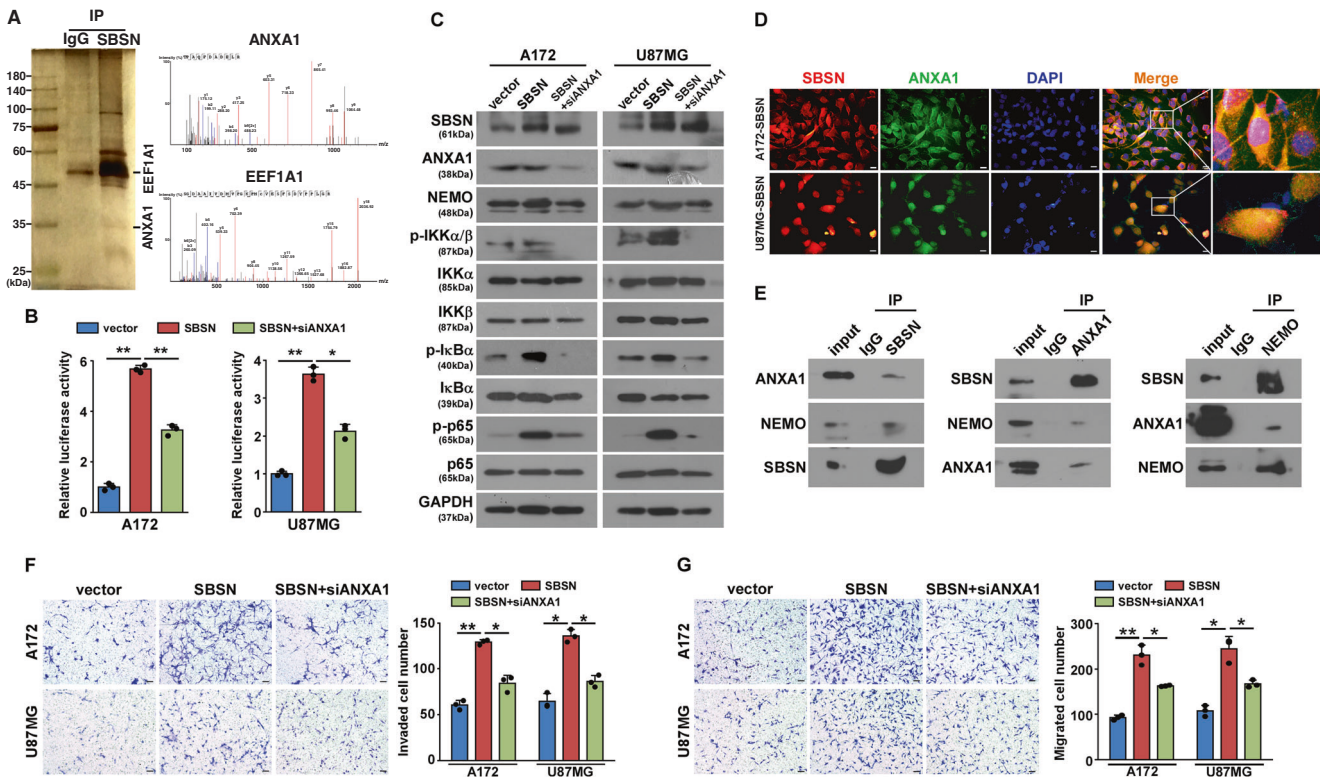


Fig. 6 EVs-transferred SBSN activates NF- κ B through ANXA1. **A** Lysates from U87MG cells transfected with SBSN were immunoprecipitated using anti-SBSN antibody. Extracts of lysates separated by 9% acrylamide SDS-PAGE and visualized by diamine silver staining, and the mass spectrometry peptide sequencing revealed the interaction between SBSN and ANXA1 or EEF1A1. **B** NF- κ B luciferase reporter activity was analyzed in the indicated cells. **C** Western blotting analysis of NF- κ B signaling-related regulatory proteins in the indicated cells. **D** Immunofluorescence staining analysis of subcellular localization of SBSN and ANXA1 in the SBSN-overexpressing glioma cells. Scale bar, 20 μ m. **E** U87MG cells transfected with SBSN plasmids, and antibodies against SBSN, ANXA1 and NEMO were used to perform co-IP. **F, G** Representative images (left) and quantification (right) of indicated invaded (**F**) and migrated (**G**) cells analyzed in a transwell matrix penetration assay. Scale bar, 20 μ m. Error bar represents the mean \pm SD of three independent experiments. * P < 0.05; ** P < 0.01.

NEMO by upregulating the expression of the LUBAC complex. This dual mechanism of NEMO ubiquitination by SBSN depends on its partner ANXA1 in glioma cells, which leads to NF- κ B-dependent tumor migration and invasion. Therefore, inhibition of NEMO linear ubiquitination can inhibit tumor growth and metastasis [45].

Tumor heterogeneity is evident not only in cancers from different patients (inter-tumor heterogeneity), but also within individual tumors (intra-tumor heterogeneity) [46]. The intra-tumor heterogeneity includes phenotypic diversity, such as cell surface markers, genetic or epigenetic abnormalities, and other hallmarks of tumor that eventually lead to disease progression and treatment failure [47]. EVs play an significant role in mediating intra-tumoral heterogeneity through multiple mechanisms [6, 7]. For example, EVs secreted by glioma cells can communicate with the component cells within the tumor microenvironment (such as astrocytes) to drive the development of tumorigenic phenotypes in astrocytes, thereby supporting the growth of the tumor itself [48]. In addition, EVs produced by glioblastoma multiforme cells can transfer immunomodulatory molecules to immune cells, thereby establishing an immunosuppressive tumor microenvironment that supports tumor growth [49, 50]. Our current research shows that glioma tissue represents a high degree of tumor heterogeneity, in which EVs-mediated transfer of SBSN from parental cells promotes the invasion and migration of recipient cells by activating NF- κ B signals, and ultimately promotes the aggressiveness of glioma. Blocking the generation or release of EVs in glioma may be a potential therapeutic strategy.

SBSN can be used as a potential prognostic biomarker for multiple cancer types [19]. Here, we demonstrated that SBSN is significantly

upregulated in glioma tissue, and is positively correlated with the increasing WHO malignancy grade of glioma. Kaplan–Meier analysis based on our own patients and two independent publicly available glioma datasets revealed that glioma patients with higher SBSN expression had shorter overall and relapse-free survivals. SBSN may also be used for the early diagnosis for patients with glioma. Since the current study analyzed a limited number of glioma samples, the clinical significance of SBSN deserves further study in a larger sample follow-up study.

CONCLUSIONS

In summary, our findings demonstrate that EVs-transferred SBSN promotes the aggressiveness of glioma by activating NF- κ B signaling that depends on ANXA1-mediated ubiquitination of NEMO. The presence of this extracellular form confers the possibility of SBSN as a noninvasive biomarker, which may facilitate early diagnosis of glioma.

METHODS AND MATERIALS

Cell culture and treatments

Glioma cells lines (LN229, LN18, T98G, U118MG, A172, U87MG, U251MG, and U138MG) were purchased from American Type Culture Collection (ATCC). Murine glioma cell line GL261 and normal human astrocytes (NHA) were purchased from Sidea Biotechnology (Guangzhou, CHN) and Bluebio (Shanghai, CHN), respectively. These cell lines were cultured in Dulbecco's modified Eagle's medium (DMEM) (Gibco, Grand Island, NY, #C11995500BT) supplemented with 10% fetal bovine serum (FBS) (Gibco, #10270-106). HUVEC was purchased from ATCC and cultured in Endothelial

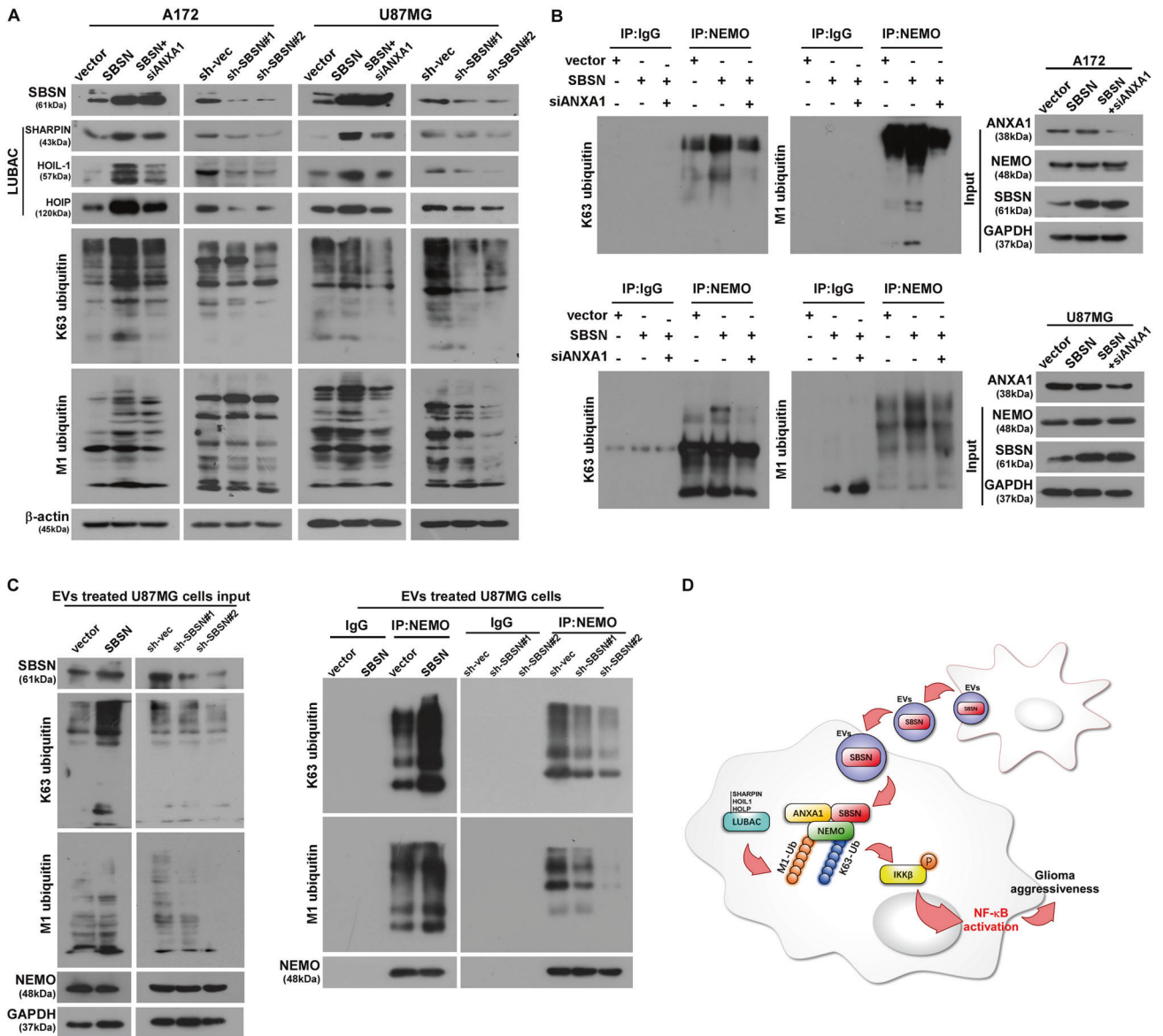


Fig. 7 EVs-transferred SBSN activates NF-κB through ANXA1-dependent NEMO ubiquitination. **A** Western blotting analysis of LUBAC, K63, M1 ubiquitin protein in the indicated cells. **B** Cell lysates of indicated cells were immunoprecipitated with anti-NEMO antibody, followed by immunoblotting with anti-K63 or anti-M1 ubiquitin antibody. **C** Cell lysates of U87MG cells treated with EVs of indicated groups were immunoprecipitated with anti-NEMO antibody, followed by immunoblotting with anti-K63 or anti-M1 ubiquitin antibody. **D** The schematic model showing that SBSN sustains NF-κB activation and consequently results in glioma aggressiveness.

Cell Medium (Sciencell, Carlsbad, CA, #1001) supplemented with 5% FBS. All cells were authenticated, tested for mycoplasma contamination, and cultured in a humidified incubator at 37 °C and 5% CO₂. NF-κB inhibitors JSH-23 (#S7351) and QNZ (#S4902) were purchased from Selleck (Houston, TX) and dissolved in DMSO. Cells were pretreated with JSH-23 and QNZ for 48 h. GW4869 (5 μM; Selleck, #S7609) was used to treat cells for 24 h and then conditioned medium was collected.

Tissue specimens

The tissue array (#HBraG177Su01) (Outdo Biotech, Shanghai, CHN) including 168 glioma tissues and six normal brain tissues was used for the detection of SBSN expression. Clinical and clinicopathological classification and grade were determined according to the guideline of the World Health Organization (WHO). According to the Diagnosis and Treatment Guidelines for Glioma (2022, National Health Commission of the People’s Republic of China), WHO grade I and II were combined as low-grade glioma, and WHO grade III and IV were combined into high-grade glioma. Normal brain tissues were obtained from individuals who died in traffic accidents and were confirmed to be free of any preexisting pathologically detectable conditions.

Prior donors’ consent and approval from the Institutional Research Ethics Committee were obtained. The clinical information on the patients’ samples is shown in Supplementary Tables 1–3.

Plasmids, RNAi, and transfection

pLent-SBSN was generated by subcloning the PCR-amplified human SBSN coding sequence (NM_001166034) into pLent-vector (Vigene Biosciences, Shandong, CHN). Glioma cells were transduced with lentivirus particles expressing SBSN or short hairpin RNAs (shRNAs) targeting the SBSN sequence (Vigene Biosciences). ANXA1-siRNA (#stB0009886A-1-5) and EE1A1-siRNA (#stB0005131A-1-5) were purchased from RiboBio (Guangzhou, CHN). Plasmids and siRNAs were transfected using Lipofectamine 3000 (Invitrogen, Carlsbad, CA, #L3000015). An SBSN-OPT construct with deletion of the signal peptide sequence of SBSN protein (Yunzhou Biosciences, Guangzhou, CHN, #VB200228-1074cqm) was used to block its secretion. Stable cell lines expressing SBSN, shRNA-SBSN or SBSN-OPT were selected for 10 days with 0.5 μg/mL puromycin (Selleck, #S9631) for 48 h after infection. All the sequences of shRNA, siRNA and SBSN-OPT construct were shown in Supplementary Table 4.

Western blotting and immunoprecipitation analysis

Cells and EVs were prepared in the RIPA lysis buffer (Cell Signaling Technology, Danvers, MA, #9806) and quantified using BCA kit (Thermo, Waltham, MA, #23227). For immunoprecipitation under denaturing conditions, harvested cells were lysed in a buffer with 1% SDS and 5 mM DTT. The samples were boiled at 95 °C for 5 minutes, then diluted into 0.1% SDS and 0.5 mM DTT with lysis buffer. The soluble supernatant fractions were harvested and subjected to immunoprecipitation experiments. The follow primary antibodies were used: SBSN (#ab232771), NEMO (#ab178872), CD63 (#ab134045) (Abcam, Cambridge, MA); p-IKK α / β (Ser176/180) (#2697), IKK α (#11930), IKK β (#8943), I κ B α (#4814), p-I κ B α (Ser32) (#2859), p65 (#8242), p-p65 (Ser536) (#4887), GAPDH (#5174), β -actin (#3700), K63 (#12930), ANXA1 (#32934), EEF1A1 (#2551), CD9 (#13403), calnexin (#2679) (Cell Signaling Technology); and M1 ubiquitin (Millipore, #MABS451). After incubation with the HRP-conjugated secondary antibody (Cell Signaling Technology, #7074, #7076), chemiluminescence signal was detected using Immobilon ECL Ultra Western HRP Substrate (Millipore, #WBULS0100). The original western blots were provided in the Supplementary material.

Tumor model and sample staining

BALB/c nude mice (female, 4–5 weeks of age, weighting 18–20 g) were purchased from Beijing Vital River Laboratory Animal Technology (Beijing, CHN). All experimental procedures were approved by the Institutional Animal Care and Use Committee of Guangzhou Medical University. BALB/c nude mice were housed in specific pathogen-free conditions and randomly divided into two groups for further implants. One group was inoculated intracranially for the orthotopic tumor model. The indicated cells (GL261-vector cells, GL261-SBSN cells, GL261-shRNA-vector cells, and GL261-shRNA-SBSN cells, 5×10^5) were stereotactically implanted into mice brains ($n = 5$, each group). The glioma-bearing mice were sacrificed two weeks later. After whole brains were removed, 6- μ m sections were cut to hematoxylin and eosin (H&E) or immunohistochemical (IHC) staining. Another group was inoculated subcutaneously with indicated cells (1×10^6) ($n = 5$, each group). Tumor growth was monitored every 5 days. Tumor volume was measured from two directions with a digital caliper and calculated as follows (length \times width²)/2. Twenty days (GL261-vector cells vs. GL261-SBSN cells-inoculated group) or 25 days (GL261-shRNA-vector cells vs. GL261-shRNA-SBSN cells-inoculated group) after tumor implantation, the mice were sacrificed and the tumors were removed and weighed. Tumors were fixed in formalin for 2 days and then embedded in paraffin using conventional method. Serial 6.0- μ m sections were cut and subjected to H&E staining, or IHC staining with SBSN, p65 or MMP9 (#10375-2-AP) (Proteintech, Rosemont, IL) antibodies. Microvascular densities (MVD) were indicated by CD31 (#11265-1-AP) (Proteintech) staining.

Transwell matrix penetration assay and transwell assay

Transwell with 8.0- μ m pore polyester membrane insert was purchased from Corning (Corning, NY, #3422). Cells (1×10^4) were planted on the top side of polycarbonate transwell filters coated with or without the Cultrex Basement Membrane Extract (BME) (R&D Systems, Minneapolis, MN, #3432-010-01) in the upper chamber of transwell and incubated at 37 °C for 24 h, followed by removal of cells inside of the upper chamber using cotton swabs. Invaded and migrated cells on the lower membrane surface were fixed in 4% paraformaldehyde (#P0099, Beyotime Biotechnology, Shanghai, CHN) for 15 min, stained with hematoxylin and counted.

EVs isolation, characterization, and treatments

EVs were purified from U87MG-derived conditioned medium. U87MG cells (1×10^6) were plated in a 100-mm dish and cultured in DMEM supplemented with 10% FBS to 70–80% confluence. The cells were then transferred to DMEM with 10% EVs-free FBS (FBS centrifuged at 110,000 g for 16 h to eliminate EVs) and the supernatants were collected after 48 h. For the small EVs isolation, the supernatants were first centrifuged at 2000 g for 10 min to remove dead cells and then remove debris at 10,000 g for 1 h. Next, the supernatants were concentrated with a 100-kDa ultrafiltration device (Millipore, #UFC910096) and filtered through 0.22- μ m filters (Millipore, #SLGP033RB) to eliminate vesicles larger than 200 nm. The resulting supernatants were centrifuged at 110,000 g for 70 min in Beckman Coulter Optima XPN-100 ultracentrifuge (Beckman Coulter, Germany) for the EV precipitates. The EV precipitates were washed with PBS (Gibco, #C10010500BT) and centrifuged for another 70 min. The final concentrations of the EVs were determined using a BCA kit (Thermo,

#23227). Generally, 100–300 μ g EVs were isolated from a total volume of 200–400 mL of the conditioned medium. Finally, the EVs were resuspended in PBS and stored at -80 °C. EV marker proteins, CD9 (Cell Signaling Technology, #13403), Calnexin (Cell Signaling Technology, #2679) and CD63 (Abcam, #ab134045) were examined by western blotting. For cell treatments, 50 μ g/mL of EVs were incubated with glioma cells for 48 h.

EVs fluorescent labeling and uptake assay

For EVs uptake experiments, EVs preparations were labeled with PKH26 Fluorescent Cell Linker Kits (Sigma-Aldrich, St. Louis, MO, #MINI26-1KT) according to the manufacturer's instructions. Briefly, the extracted EV pellets were resuspended in 1 mL Diluent C (1 mL Diluent C was mixed with 6 μ L PKH26). The EVs suspension was mixed with the stain solution and incubated for 5 min at room temperature, while the PBS without EVs mixed with the stain solution was used as the PKH26 dye-fluorescence background control (shown as PBS-PKH26). The labeling reaction was stopped by adding 2 mL PBS which contain 0.5% BSA. Labeled EVs were ultracentrifuged at 100,000 g for 90 min, washed with PBS, and ultracentrifuged again. Next, the fluorescent labeled EVs were incubated with U87MG cells for 48 h. The U87MG cells were stained with 4'-diamidino-2-phenylindole (DAPI) and observed under an inverted fluorescence microscope to determine whether U87MG cells could endocytose the EVs. Images were obtained using an inverted fluorescence microscope (Carl Zeiss, Oberkochen).

EVs-transferred protein uptake assay

To determine whether EVs transfer protein into the target cells, the XPack Exosome Protein Engineering Technology was used according to the manufacturer's instructions (System Biosciences, SBI, CA, #XPAK730PA-1). To generate EVs containing high levels of SBSN, the open reading frame sequence for SBSN was cloned the downstream of XPack-peptide in the XPack-cloning lentivector, which can produce lentiviral particles for the establishment of stable cell lines. The XPack stable cell lines continuously secreted EVs containing reporter protein TurboGFP and the purified EVs from XPack stable cell lines were ready for addition to target U87MG cells. 50 μ g/mL of EVs containing XPack-vector-TurboGFP or XPack-SBSN-TurboGFP were added to target cells and the cells were imaged on a confocal microscope 24 h after EVs addition.

Statistical analysis

Data were analyzed statistically by using Fisher's exact test, log-rank test, χ^2 test, or Student's two-tailed *t*-test. The receiver-operating characteristics (ROC) curve was used to determine the diagnostic value of SBSN expression in patients with glioma. The construction of the ROC curves was performed using GraphPad Prism and the areas under ROC curve (AUC) with 95% confidence interval (CI) was calculated to evaluate the diagnostic accuracy and discrimination power. Survival curves were plotted by the log-rank test. The pathway and function gene expression signatures were analyzed using Gene Set Enrichment Analysis (GSEA) [51, 52]. For each sample and signature, GSEA reported a signature expression score between 0 and 1 and the statistical significance (*P* value) for signature overexpression. GraphPad Prism and Excel software were used for statistical analysis. All experiments were performed at least three times, and $P \leq 0.05$ was considered statistically significant.

DATA AVAILABILITY

For survival analysis of glioma patients, the Chinese Glioma Genome Atlas (CGGA) and the Cancer Genome Atlas (TCGA) datasets were used. All other data supporting the findings of this study are available within the article and its Supplementary information files and on reasonable request from the corresponding author.

REFERENCES

- Lapointe S, Perry A, Butowski NA. Primary brain tumours in adults. *Lancet*. 2018;392:432–46.
- Delgado-Lopez PD, Corrales-Garcia EM. Survival in glioblastoma: a review on the impact of treatment modalities. *Clin Transl Oncol*. 2016;18:1062–71.
- Alexander BM, Cloughesy TF. Adult glioblastoma. *J Clin Oncol*. 2017;35:2402–09.
- Wortzel I, Dror S, Kenific CM, Lyden D. Exosome-mediated metastasis: communication from a distance. *Dev Cell*. 2019;49:347–60.

5. Mathieu M, Martin-Jaular L, Lavieu G, Thery C. Specificities of secretion and uptake of exosomes and other extracellular vesicles for cell-to-cell communication. *Nat Cell Biol.* 2019;21:9–17.
6. Thery C, Zitvogel L, Amigorena S. Exosomes: composition, biogenesis and function. *Nat Rev Immunol.* 2002;2:569–79.
7. Liu Y, Ye G, Huang L, Zhang C, Sheng Y, Wu B, et al. Single-cell transcriptome analysis demonstrates inter-patient and intra-tumor heterogeneity in primary and metastatic lung adenocarcinoma. *Aging (Albany NY).* 2020;12:21559–81.
8. Becker A, Thakur BK, Weiss JM, Kim HS, Peinado H, Lyden D. Extracellular vesicles in cancer: cell-to-cell mediators of metastasis. *Cancer Cell.* 2016;30:836–48.
9. Cheng J, Meng J, Zhu L, Peng Y. Exosomal noncoding RNAs in Glioma: biological functions and potential clinical applications. *Mol Cancer.* 2020;19:66.
10. Gao X, Zhang Z, Mashimo T, Shen B, Nyagilo J, Wang H, et al. Gliomas interact with non-glioma brain cells via extracellular vesicles. *Cell Rep.* 2020;30:2489–500 e5.
11. Zhang Q, Lenardo MJ, Baltimore D. 30 Years of NF-kappaB: a blossoming of relevance to human pathobiology. *Cell.* 2017;168:37–57.
12. Hayden MS, Ghosh S. NF-kappaB, the first quarter-century: remarkable progress and outstanding questions. *Genes Dev.* 2012;26:203–34.
13. Karin M. Nuclear factor-kappaB in cancer development and progression. *Nature.* 2006;441:431–6.
14. Taniguchi K, Karin M. NF-kappaB, inflammation, immunity and cancer: coming of age. *Nat Rev Immunol.* 2018;18:309–24.
15. Cahill KE, Morshed RA, Yamini B. Nuclear factor-kappaB in glioblastoma: insights into regulators and targeted therapy. *Neuro Oncol.* 2016;18:329–39.
16. Chen J, Chen ZJ. Regulation of NF-kappaB by ubiquitination. *Curr Opin Immunol.* 2013;25:4–12.
17. Hinz M, Scheidereit C. The IkkappaB kinase complex in NF-kappaB regulation and beyond. *EMBO Rep.* 2014;15:46–61.
18. Park GT, Lim SE, Jang SI, Morasso MI. Suprabasin, a novel epidermal differentiation marker and potential cornified envelope precursor. *J Biol Chem.* 2002;277:45195–202.
19. Pribyl M, Hodny Z, Kubikova I. Suprabasin—a review. *Genes (Basel).* 2021;12:108.
20. Matsui T, Hayashi-Kisumi F, Kinoshita Y, Katahira S, Morita K, Miyachi Y, et al. Identification of novel keratinocyte-secreted peptides dermokine-alpha/-beta and a new stratified epithelium-secreted protein gene complex on human chromosome 19q13.1. *Genomics.* 2004;84:384–97.
21. Pribyl M, Hubackova S, Moudra A, Vancurova M, Polackova H, Stopka T, et al. Aberrantly elevated suprabasin in the bone marrow as a candidate biomarker of advanced disease state in myelodysplastic syndromes. *Mol Oncol.* 2020;14:2403–19.
22. Aoshima M, Phadungsaksawasdi P, Nakazawa S, Iwasaki M, Sakabe JI, Umayahara T, et al. Decreased expression of suprabasin induces aberrant differentiation and apoptosis of epidermal keratinocytes: possible role for atopic dermatitis. *J Dermatol Sci.* 2019;95:107–12.
23. Yanovich-Arad G, Ofek P, Yeini E, Mardamshina M, Danilevsky A, Shomron N, et al. Proteogenomics of glioblastoma associates molecular patterns with survival. *Cell Rep.* 2021;34:108787.
24. Lauko A, Lo A, Ahluwalia MS, Lathia JD. Cancer cell heterogeneity & plasticity in glioblastoma and brain tumors. *Semin Cancer Biol.* 2022;82:162–75.
25. Zomer A, Maynard C, Verweij FJ, Kamermans A, Schafer R, Beerling E, et al. In vivo imaging reveals extracellular vesicle-mediated phenocopying of metastatic behavior. *Cell.* 2015;161:1046–57.
26. Raposo G, Stoorvogel W. Extracellular vesicles: exosomes, microvesicles, and friends. *J Cell Biol.* 2013;200:373–83.
27. Raychaudhuri B, Han Y, Lu T, Vogelbaum MA. Aberrant constitutive activation of nuclear factor kappaB in glioblastoma multiforme drives invasive phenotype. *J Neurooncol.* 2007;85:39–47.
28. Ji J, Ding K, Luo T, Zhang X, Chen A, Zhang D, et al. TRIM22 activates NF-kappaB signaling in glioblastoma by accelerating the degradation of IkkappaBalpha. *Cell Death Differ.* 2021;28:367–81.
29. Wang SS, Feng L, Hu BG, Lu YF, Wang WM, Guo W, et al. miR-133a promotes TRAIL resistance in glioblastoma via suppressing death receptor 5 and activating NF-kappaB signaling. *Mol Ther Nucleic Acids.* 2017;8:482–92.
30. Srivastava C, Irshad K, Gupta Y, Sarkar C, Suri A, Chattopadhyay P, et al. NFkappaB is a critical transcriptional regulator of atypical cadherin FAT1 in glioma. *BMC Cancer.* 2020;20:62.
31. Sarkar S, Yong VW. Inflammatory cytokine modulation of matrix metalloproteinase expression and invasiveness of glioma cells in a 3-dimensional collagen matrix. *J Neurooncol.* 2009;91:157–64.
32. Bond M, Fabunmi RP, Baker AH, Newby AC. Synergistic upregulation of metalloproteinase-9 by growth factors and inflammatory cytokines: an absolute requirement for transcription factor NF-kappa B. *FEBS Lett.* 1998;435:29–34.
33. Wei S, Wang D, Li H, Bi L, Deng J, Zhu G, et al. Fatty acylCoA synthetase FadD13 regulates proinflammatory cytokine secretion dependent on the NF-kappaB signalling pathway by binding to eEF1A1. *Cell Microbiol.* 2019;21:e13090.
34. Bist P, Leow SC, Phua QH, Shu S, Zhuang Q, Loh WT, et al. Annexin-1 interacts with NEMO and RIP1 to constitutively activate IKK complex and NF-kappaB: implication in breast cancer metastasis. *Oncogene.* 2011;30:3174–85.
35. Wu Y, Kang J, Zhang L, Liang Z, Tang X, Yan Y, et al. Ubiquitination regulation of inflammatory responses through NF-kappaB pathway. *Am J Transl Res.* 2018;10:881–91.
36. Song K, Cai X, Dong Y, Wu H, Wei Y, Shankavaram U, et al. Epsins 1 and 2 promote NEMO linear ubiquitination via LUBAC to drive breast cancer development. *J Clin Invest.* 2020;131:e129374.
37. Rahighi S, Ikeda F, Kawasaki M, Akutsu M, Suzuki N, Kato R, et al. Specific recognition of linear ubiquitin chains by NEMO is important for NF-kappaB activation. *Cell.* 2009;136:1098–109.
38. Wertz IE, Dixit VM. Signaling to NF-kappaB: regulation by ubiquitination. *Cold Spring Harb Perspect Biol.* 2010;2:a003350.
39. Chen ZJ, Sun LJ. Nonproteolytic functions of ubiquitin in cell signaling. *Mol Cell.* 2009;33:275–86.
40. Yamamoto M, Okamoto T, Takeda K, Sato S, Sanjo H, Uematsu S, et al. Key function for the Ubc13 E2 ubiquitin-conjugating enzyme in immune receptor signaling. *Nat Immunol.* 2006;7:962–70.
41. Ea CK, Deng L, Xia ZP, Pineda G, Chen ZJ. Activation of IKK by TNFalpha requires site-specific ubiquitination of RIP1 and polyubiquitin binding by NEMO. *Mol Cell.* 2006;22:245–57.
42. Lee IY, Lim JM, Cho H, Kim E, Kim Y, Oh HK, et al. MST1 negatively regulates TNFalpha-induced NF-kappaB signaling through modulating LUBAC activity. *Mol Cell.* 2019;73:1138–49.e6.
43. Tokunaga F, Sakata S, Saeki Y, Satomi Y, Kirisako T, Kamei K, et al. Involvement of linear polyubiquitylation of NEMO in NF-kappaB activation. *Nat Cell Biol.* 2009;11:123–32.
44. Yang Y, Schmitz R, Mitala J, Whiting A, Xiao W, Ceribelli M, et al. Essential role of the linear ubiquitin chain assembly complex in lymphoma revealed by rare germline polymorphisms. *Cancer Disco.* 2014;4:480–93.
45. Niu J, Shi Y, Iwai K, Wu ZH. LUBAC regulates NF-kappaB activation upon genotoxic stress by promoting linear ubiquitination of NEMO. *EMBO J.* 2011;30:3741–53.
46. Prasetyanti PR, Medema JP. Intra-tumor heterogeneity from a cancer stem cell perspective. *Mol Cancer.* 2017;16:41.
47. Gerlinger M, Rowan AJ, Horswell S, Math M, Larkin J, Endesfelder D, et al. Intra-tumor heterogeneity and branched evolution revealed by multiregion sequencing. *N. Engl J Med.* 2012;366:883–92.
48. Oushy S, Hellwinkel JE, Wang M, Nguyen GJ, Gunaydin D, Harland TA, et al. Glioblastoma multiforme-derived extracellular vesicles drive normal astrocytes towards a tumour-enhancing phenotype. *Philos Trans R Soc Lond B Biol Sci.* 2018;373:20160477.
49. Abels ER, Broekman MLD, Breakefield XO, Maas SLN. Glioma EVs contribute to immune privilege in the brain. *Trends Cancer.* 2019;5:393–96.
50. de Vrij J, Maas SL, Kwappenberg KM, Schnoor R, Kleijn A, Dekker L, et al. Glioblastoma-derived extracellular vesicles modify the phenotype of monocytic cells. *Int J Cancer.* 2015;137:1630–42.
51. Subramanian A, Tamayo P, Mootha VK, Mukherjee S, Ebert BL, Gillette MA, et al. Gene set enrichment analysis: a knowledge-based approach for interpreting genome-wide expression profiles. *Proc Natl Acad Sci USA.* 2005;102:15545–50.
52. Mootha VK, Lindgren CM, Eriksson KF, Subramanian A, Sihag S, Lehar J, et al. PGC-1alpha-responsive genes involved in oxidative phosphorylation are coordinately downregulated in human diabetes. *Nat Genet.* 2003;34:267–73.

AUTHOR CONTRIBUTIONS

LJ and JL developed the original idea, designed the study, analyzed data, and wrote the manuscript. HC, XC, ZZ and WB contributed to the development of the protocol and performed most of the experiments and data analysis. ZG, DL, XX, PZ, CY and ZZ contributed to the in vitro biological experiments and data analysis. HC, ZZ, ZG and XX performed the in vivo experiments and data analysis. ZZ, JP, XK, DZ, JY and LW contributed to clinical data collection and statistical analysis. RT, ZF, LZ and HH provided the bioinformatics analysis. DT assisted in data interpretation and edited the manuscript.

FUNDING

This work was supported by the Basic and Applied Research Projects of Guangzhou Science and Technology Bureau (202002030067), the Natural Science Foundation of

China (82273464, 81972619, 81672874, and 81972399), the Natural Science Foundation of Guangdong Province (2021A1515012477 and 2022A1515012260), the Key Discipline of Guangzhou Education Bureau (Basic Medicine) (201851839), the Natural Science Foundation research team of Guangdong Province (2018B030312001), the open research funds from the Sixth Affiliated Hospital of Guangzhou Medical University, Qingyuan People's Hospital (202011-202), the Innovative Academic Team of Guangzhou Education System (1201610014), and the Guangzhou key medical discipline construction project fund.

COMPETING INTERESTS

The authors declare no competing interests.

ETHICS APPROVAL AND CONSENT TO PARTICIPATE

Investigation has been conducted in accordance with the ethical standards according to the Declaration of Helsinki and national and international guidelines and has been approved by the authors' Institutional Review Board.

ADDITIONAL INFORMATION

Supplementary information The online version contains supplementary material available at <https://doi.org/10.1038/s41388-022-02520-6>.

Correspondence and requests for materials should be addressed to Jinbao Liu or Lili Jiang.

Reprints and permission information is available at <http://www.nature.com/reprints>

Publisher's note Springer Nature remains neutral with regard to jurisdictional claims in published maps and institutional affiliations.

Springer Nature or its licensor (e.g. a society or other partner) holds exclusive rights to this article under a publishing agreement with the author(s) or other rightsholder(s); author self-archiving of the accepted manuscript version of this article is solely governed by the terms of such publishing agreement and applicable law.